Cement and Concrete Composites 115 (2021) 103787

Contents lists available at ScienceDirect

Cement and Concrete Composites

journal homepage: http://www.elsevier.com/locate/cemconcomp

Experimental analysis and modelling of mechanical properties and shrinkage of concrete recycling flash calcined dredging sediments

Céline Van Bunderen [a,*], Farid Benboudjema [b], Ruben Snellings [c], Lucie Vandewalle [a], Özlem Cizer [a]

[a] Department of Civil Engineering, KU Leuven, Leuven, Belgium
[b] LMT, ENS Paris-Saclay, CNRS, Université Paris-Saclay, Cachan, France
[c] Sustainable Materials Management, VITO, Mol, Belgium

ARTICLE INFO

Keywords:
Calcined dredging sediments
Mechanical properties
Autogenous shrinkage models
Drying shrinkage models

ABSTRACT

This paper aims to assess the influence of calcined dredging sediments (CFC) from Antwerp port as a new SCM on the mechanical properties and shrinkage behaviour of concrete, where cement is replaced by 20, 30 and 40 wt% of CFC. Experimental results are compared with the current prediction models. CFC blended cement develops lower cumulative heat, compared to an OPC reference mix, resulting in a lower temperature development. Although the strength development of a CFC concrete mix is slower than that of an OPC reference mix, CFC concrete reaches higher compressive strength values after 28 days. Both autogenous and total shrinkage are reduced by using CFC blended cement. The development of the mechanical properties can be well described using the model from Eurocode 2, provided that the cement type dependent parameters were adjusted according to the new blended cement system. The existing shrinkage prediction models are also parametrised. All considered drying shrinkage models describe well the drying shrinkage development, while for autogenous shrinkage, the Bazant B4 model appears to be the best predictor. The results clearly support the use of CFC as a new SCM for the production of sustainable cement and concrete.

1. Introduction

As the world's largest manufactured product by mass, cement is responsible for 10% of the total anthropogenic CO_2 emissions, or about 6% of the total anthropogenic greenhouse gases [1]. Due to the rapid population growth in developing countries and the enormous growth in cement demand associated with it, the share of the cement production in the global CO_2 emissions is only expected to increase [1,2]. The biggest challenge of the cement industry nowadays is therefore the reduction of these emissions, in order to contribute to achieving the United Nations sustainable development goals [3]. An important and well-established way to do so is by using supplementary cementitious materials (SCMs) as partial cement replacement in concrete. The average clinker-to-cement ratio currently equals around 73.7% [4], however, there is a limited potential for further reduction, since the supply of the most desirable high-quality SCMs (i.e. fly ash and blast furnace slag) is decreasing [1,5,6]. This proves the need for new alternative sources of SCMs.

The utilisation of calcined clays as a pozzolanic material for concrete has received considerable interest in recent years, as a part of the more widely spread attention towards the use of wastes, locally available minerals and industrial by-products as alternative SCMs [2,7]. Calcined dredging sediments, initially containing a considerable amount of clay minerals, are a promising new SCM for use in concrete [8–15]. Dredging sediments are generated in large quantities. In the port of Antwerp, Belgium, only about 450.000 tons dry matter of dredging sediments is generated each year, while for Europe the yearly amount of dredging sediments is estimated at 300 million tons. At present dredging sediments are mostly disposed of in marine repositories or landfilled, causing a negative impact on the environment [16]. The beneficial reuse of this dredging material as an SCM could thus provide a sustainable solution, limiting landfilled waste and limiting extraction of natural resources [13].

Several researchers have already studied the recycling of calcined dredging sediments to replace a portion of the raw materials in the production of Portland cement or as an SCM in concrete. Most studies

* Corresponding author.
E-mail address: celine.vanbunderen@gmail.com (C. Van Bunderen).

https://doi.org/10.1016/j.cemconcomp.2020.103787
Received 27 September 2019; Received in revised form 27 July 2020; Accepted 18 August 2020
Available online 28 September 2020

have focused on the characterisation of the dredging sediments and their behaviour in cement pastes and mortars [8,10,12–14]. The properties, pozzolanic reactivity and hydration process of the calcined dredging sediments from the port of Antwerp (henceforth called 'calcined filter cakes' or CFC), were intensively investigated by the authors [12,14,15]. In order to assess the performance of concrete with CFC and predict the serviceability and durability of a concrete structure, analysis of the mechanical properties development and shrinkage behaviour, and prediction of the time-dependent deformations (regarding associated cracking risk) of the concrete are required. Only few studies have investigated fresh and hardened (mechanical) properties of concrete with calcined dredging sediments [9,11] and very limited research has been performed regarding concrete shrinkage behaviour [11]. The aim of this study therefore is twofold. The first objective is to study the influence of the addition of CFC on the mechanical properties development and shrinkage behaviour of concrete, by experimental analysis. The second objective is to assess the accuracy of existing mechanical properties and shrinkage prediction models for the CFC blended cement concretes. Finally, the behaviour of CFC is compared to the behaviour of a commonly used SCM: siliceous coal combustion fly ash.

The development of the mechanical properties is predicted using the model from Eurocode 2 [17]. This model is parameterised in order to include the addition effect of CFC and different fitting methods are used in order to validate the Eurocode 2 model. The shrinkage behaviour of concrete is mostly predicted using empirical/phenomenological models recommended by design codes. These models allow the extrapolation of experimental data and the estimation of the shrinkage magnitude and shrinkage rate. The most popular prediction models are: the CEB-FIP Model Code 2010 model [18], the Eurocode 2 model [17], the ACI 209 model [19], the JSCE 2007 model [20] (all design code models), the Gardner/Lockman GL2000 model [21] and the Bazant B4 model [22] (academic models). These models all vary in precision, complexity and parameters necessary for the calculation, and are all primarily based on pure Portland cement concrete, without considering the systematic inclusion effect of SCMs. In order to take this effect into account, the existing shrinkage prediction models need to be parameterised. Li (2016) [23] modified two existing drying shrinkage prediction models to take into account the inclusion of metakaolin and fly ash in the cement matrix, based on a regression equation for predicting the ultimate drying shrinkage. Abdalhmid et al. (2019) [24] assessed the robustness of the existing shrinkage prediction models by studying the influence of different parameters on the drying shrinkage strain of concrete with addition of fly ash. Also Mokarem et al. (2005) [25] assessed the accuracy of the existing shrinkage prediction models for concrete including various SCMs. In this study, the cement type dependent parameters of different existing shrinkage models are adjusted to take into account the addition effect of CFC and fly ash. Moreover, comparisons between the models are systematically made in order to select the best predictive one.

2. Materials and methods

2.1. Materials

CEM I 52.5 N (ordinary Portland cement) and CEM II/B–V 42.5 N (Portland cement containing 21–35% of fly ash (FA)) are used as two reference cements. The dredging sediments from the port of Antwerp are used as an alternative SCM. Properties and pozzolanic reactivity of the flash-calcined dredging sediments can be found in Refs. [12,14,15] and the treated material is henceforth called CFC (calcined filter cakes). The chemical composition of both cements and CFC is shown in Table 1. CFC is mainly composed of SiO_2, besides the other major components of CaO, Al_2O_3 and Fe_2O_3. The major mineral phases of the dredging sediments comprise clays (2:1 clays and kaolinite), quartz, calcite and an amorphous phase. Flash calcination results in a dehydroxylation of the clay minerals and decarbonation of the calcite. The dehydroxylated clay minerals react with part of the free lime released to form an amorphous reactive phase (± 50 wt%), responsible for the pozzolanic reactivity. CFC was found to be less reactive than metakaolin, but more reactive than siliceous fly ash [12]. The BET specific surface areas of CEM I, CEM II and CFC equal respectively 0.93 m^2/g, 2.20 m^2/g and 4.94 m^2/g. The mean particle size diameter (d_{50}) of CFC equals 16.8 μm (compared to 13.7 μm for OPC). Since the particle size distributions of CFC and OPC are about the same, the higher specific surface area of CFC means an increase in particle surface roughness (compared to OPC), negatively influencing its water demand.

Natural river sand 0/4 and river gravel 4/14 were used as dry aggregates and a PCE superplasticizer (Viscocrete ®-4035 M) was added to all concrete mixtures, in order to control the workability. The superplasticizer has a dry matter content of 35 ± 1.0% and a density of 1.08 ± 0.01 kg/l.

2.2. Mix design

Five different concrete compositions, including two reference mixes and three CFC blended cement mixtures, were studied. The reference mixes (RC I and RC II) were produced by using respectively CEM I 52.5 N and CEM II/B–V 42.5 N. The three blended cement mixtures (CFC 20, CFC 30 and CFC 40) were made by replacing OPC with respectively 20, 30 and 40 wt% CFC. The mix compositions of the studied concretes are shown in Table 2. The W/B ratio was kept constant as 0.45 and a PCE superplasticizer was added in order to keep the workability of the fresh concrete mixes also constant. A slump class S2 was targeted and the dosage of superplasticizer was determined experimentally, by means of trial and error testing. Both the slump values, as well as the air content of the different fresh concrete mixes can also be found in Table 2. It is observed that no superplasticizer was needed for the reference mix with fly ash (RC II), since the spherical shape and glassy surface of the fly ash particles permit sufficient workability [26,27]. The amount of superplasticizer of the CFC blended cement mixes, on the other hand, had to be increased for increasing amount of CFC, due to the high specific

Table 2
Mix proportions of the concrete mixtures.

		RC I	RC II	CFC 20	CFC 30	CFC 40
Sand 0/4	[kg/m^3]	640	640	640	640	640
Gravel 4/14	[kg/m^3]	1225	1225	1225	1225	1225
CEM I 52.5 N	[kg/m^3]	360	–	288	252	216
CEM II/B–V 42.5 N	[kg/m^3]	–	360	–	–	–
CFC	[kg/m^3]	–	–	72	108	144
Water	[l/m^3]	162	162	162	162	162
Superplasticizer	[wt. %/B]	0.35	0.20	0.55	0.70	0.75
W/B	[−]	0.45	0.45	0.45	0.45	0.45
Slump	[mm]	40	80	40	90	60
Air content	[%]	2.6	2.4	1.8	2.4	2.3

Table 1
Chemical composition [wt.%] of the cementitious materials.

	Al_2O_3	SiO_2	Fe_2O_3	CaO	MgO	Na_2O	K_2O	P_2O_5	LOI
CEM I	4.9	14.0	2.8	57.4	1.6	0.5	0.9	0.3	2.7
CEM II	11.3	22.0	4.0	45.2	1.8	0.9	1.5	0.6	2.2
CFC	13.0	42.0	9.7	12.5	2.2	1.4	3.4	0.8	1.7

surface area of the CFC particles.

2.3. Test methods

2.3.1. Heat of hydration

The heat flow of the concrete mixtures was measured using an isothermal heat conduction calorimeter (3 channel TAM AIR). Samples of 140 ± 5 g of concrete were taken at the end of mixing and the first measurements were acquired less than 10 min after the first contact between water and cement.

2.3.2. Mechanical properties

Both the compressive strength, tensile splitting strength and static elastic modulus were investigated according to the European standards, using three test specimens for each testing age. Compressive strength of the concrete mixes was determined on cubes (150 × 150 × 150 mm) according to EN 12390–3. Strength measurements were performed at early ages (12 h, 24 h and 48 h after mixing) and after 7, 28 and 90 days. Tensile splitting strength was determined according to EN 12390–6 on cylindrical specimens (ϕ150 × 300 mm) after 1, 2 and 7 days. From the tensile splitting strength ($f_{ct,sp}$), the tensile strength (f_{ct}) can be derived as [17]:

$$f_{ct} = 0.9 \cdot f_{ct,sp} \quad (1)$$

The static elastic modulus finally, was determined according to EN 12390–13 on cylindrical specimens (ϕ150 × 300 mm) after 1, 2 and 7 days.

2.3.3. Autogenous shrinkage

The autogenous shrinkage strains of the studied concretes were measured using a BTJADE device (see Fig. 1). This device is developed by Boulay [28] and is specially designed for autogenous shrinkage measurements of concrete at early ages. The test rig is composed of a flexible corrugated PVC mould - in which the concrete is cast - and a steel frame with fixed metallic parts. The whole frame is placed in a thermo-controlled bath to keep a constant temperature of 20 °C and a stress free state. A thermocouple is inserted into the concrete specimen to continuously measure the temperature inside the sample and the strains are measured by an external linear displacement sensor. The water temperature and temperature of the air above the cover of the tank are also continuously monitored. This allows calculating the 'actual' autogenous strains (ε_{au}) as the measured strains (ε_{meas}) minus the thermal strains (ε_{th}), minus the strains as a result of the temperature variation around the sensor (ε_{ts}), minus the strains resulting from the reaction of the frame (ε_{tm}):

$$\varepsilon_{au} = \varepsilon_{meas} - \varepsilon_{th} - \varepsilon_{ts} - \varepsilon_{tm} \quad (2)$$

The reported autogenous shrinkage results are the average values of two measurements on two different batches of concrete.

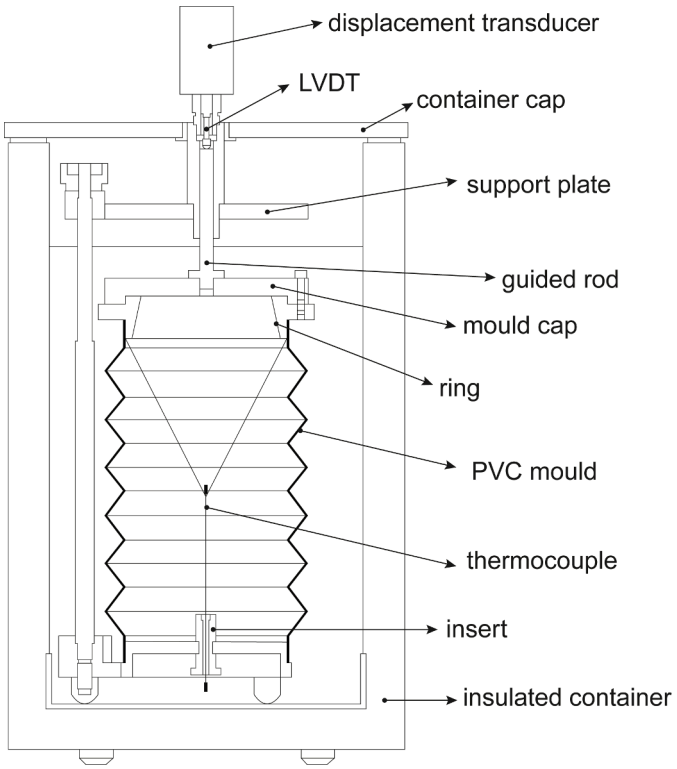

Fig. 1. BTJADE device, adapted from Ref. [29].

2.3.4. Total shrinkage

Drying shrinkage measurements were performed on cylindrical concrete specimens with a diameter of 120 mm and a height of 300 mm. A schematic overview of the drying shrinkage set-up is shown in Fig. 2, adapted from Ref. [30]. The specimens are installed in a frame made of brass, where a bottom ring is immovably fixed to the concrete specimen by means of three points, while an upper ring is only fixed in two opposite points, allowing the ring to rotate around the axis formed by the two fixation points. The two rings are connected to each other at two sides. At one side by a small bar and a spring (to keep the bar under pressure), in order to provide a fixed distance between the two rings at this side. At the other side by a second bar, holding at one end the core of an LVDT (Linear Variable Differential Transducer), in order to measure the relative displacement between the two rings. The time-dependent strains are then continuously measured by means of LVDT's and the concrete strains are then calculated as:

$$\varepsilon_{sh} = \frac{1}{2} \cdot \frac{\delta_t - \delta_0}{L_0} \quad (3)$$

with L_0 the LVDT measuring base (= 200 mm) and δ_t and δ_0 respectively the LVDT reading at time t and at the start of drying (= 1 day) [30]. The reported results are the average values of measurements on three cylinders.

3. Results and discussion

3.1. Heat of hydration

The results of the calorimetry measurements are shown in Fig. 3 and Fig. 4. The heat flow and cumulative heat of the concrete mixes follow

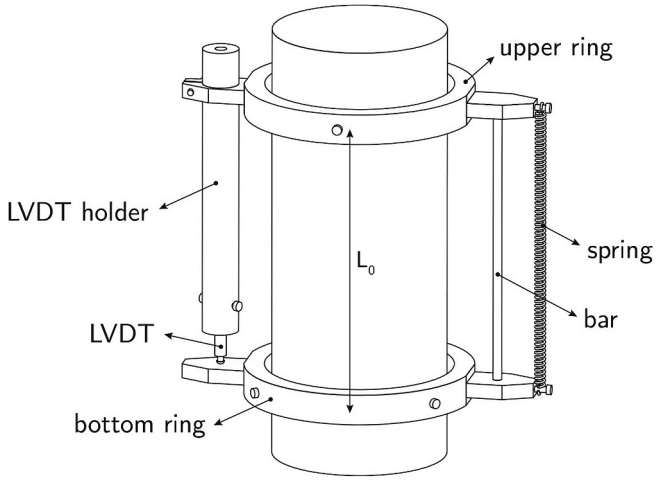

Fig. 2. Drying shrinkage set-up.

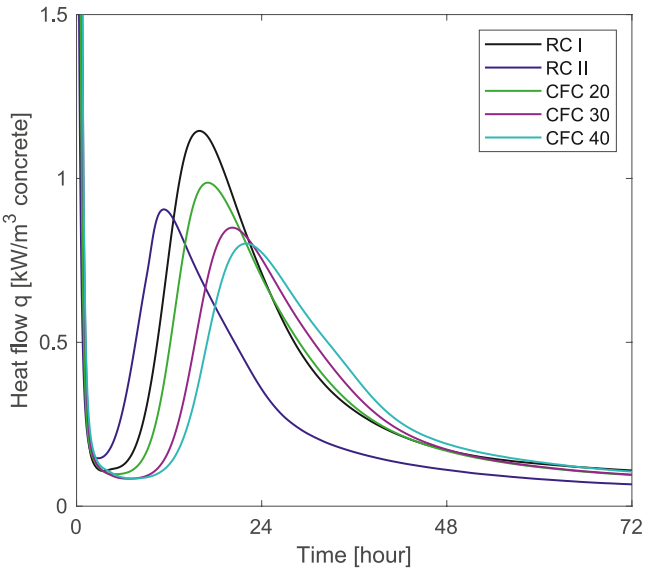

Fig. 3. Heat flow of the different concrete mixes.

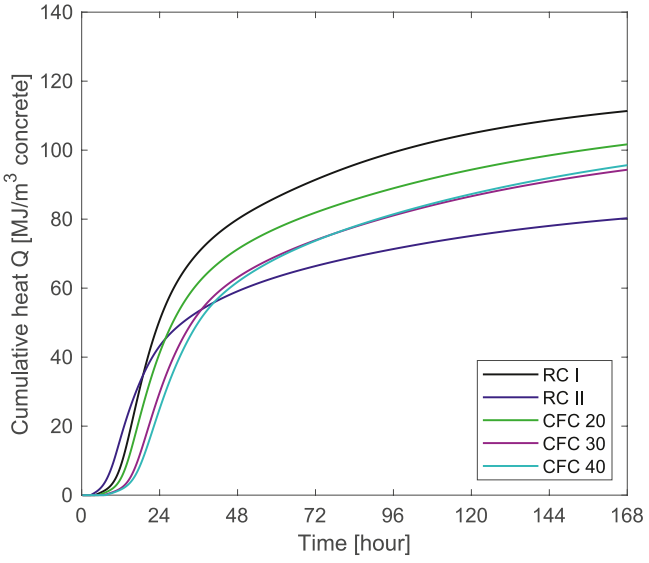

Fig. 4. Cumulative heat development of the different concrete mixes up to 7 days.

the same trend as the cement paste results [15]. Addition of CFC and FA results in a lower hydration peak, due to the dilution effect. The hydration of the CFC mixes is also delayed compared to the hydration of both reference mixes. This retardation, however, is not caused by the presence of CFC, but by the addition of the PCE superplasticizer, delaying the cement hydration proportional to the added amount [15]. Addition of more superplasticizer thus results in a stronger retardation of the cement hydration. From Fig. 4 it is clear that the replacement ratio of CFC has almost no influence on the cumulative heat development and that for the CFC mixes more cumulative heat is released compared to the reference mix with fly ash (RC II), but less compared to the OPC reference mix (RC I).

3.2. Mechanical properties

The average results of the compressive strength, tensile strength and static Young's modulus are shown in Figs. 5–7, with the error bars indicating the standard deviation. After 12 h (0.5 day), the CFC blended cement mixes show the lowest compressive strength (Fig. 5). This can be explained by the higher amount of superplasticizer, delaying the setting to more than 12 h after casting. From 1 day up to 7 days, the compressive strength of the CFC blended cement mixes notably increases, surpassing the compressive strength of the fly ash cement concrete (RC II) and from 28 days on, overtaking even the compressive strength of the OPC

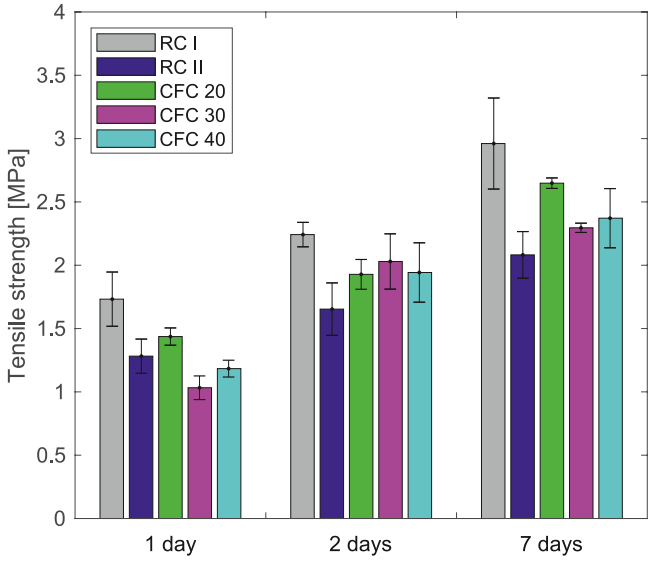

Fig. 6. Tensile strength development of the different concrete mixes up to 7 days.

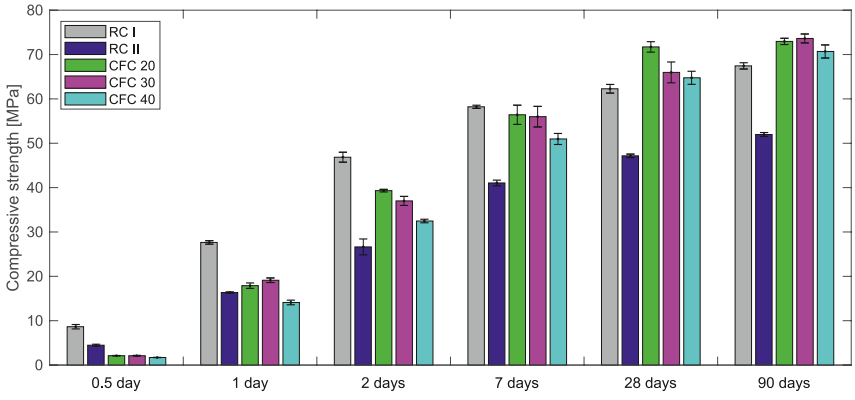

Fig. 5. Compressive strength development of the different concrete mixes up to 90 days.

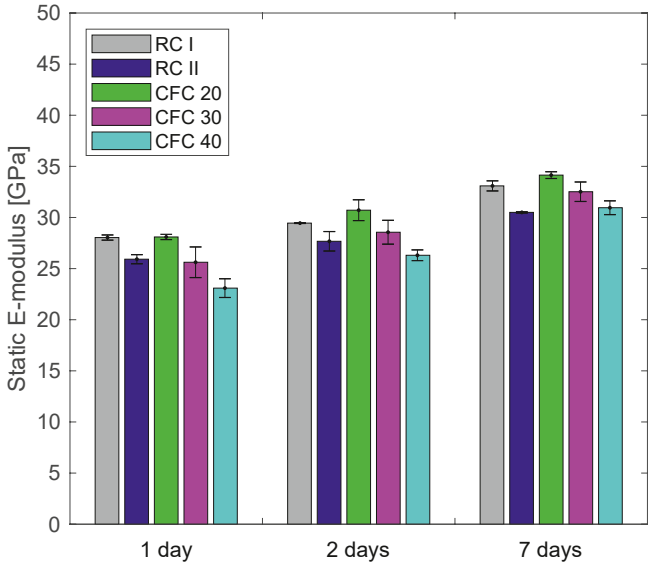

Fig. 7. Static E-modulus development of the different concrete mixes up to 7 days.

reference mix (RC I). The filler effect and pozzolanic reaction of CFC explain this behaviour. A slightly lower compressive strength for higher replacement levels of CFC is also visible, however, this difference is negligible at later ages. For the tensile strength (Fig. 6) the same general trends are visible. However, no relationship between the amount of CFC and the tensile strength can be observed. This is the result of the higher standard deviations of the tensile strength results, compared to the compressive strength results, making it difficult to observe any trend. These deviations can be explained by the indirect character of the tensile splitting strength test and the heterogeneity of the concrete specimens. The static E-modulus (Fig. 7), on the other hand, shows a faster development and less differences are observed between the different mixes.

3.3. Autogenous shrinkage

The average autogenous shrinkage strains, measured with the BTJADE device, are shown in Fig. 8, plotted from final setting. The final setting time was determined based on ultrasonic measurements, using the δE_d^{max} criteria from Ref. [31]. Negative values in Fig. 8 correspond to contraction/shrinkage of the concrete specimen, while positive values correspond to dilation/swelling. At early ages (< 24 h), the autogenous shrinkage of the CFC mixes is slightly higher than the autogenous shrinkage of the reference mixes. This is most probably due to the slower hydration and slower development of a solid matrix of the CFC mixes. However, from 24 h on, the addition of CFC clearly results in a decrease of the autogenous shrinkage by self-desiccation, compared to the OPC reference mix (RC I). Compared to the reference mix with fly ash (RC II), the shrinkage behaviour of CFC is quite similar. The lower shrinkage of the blended cement concretes can be explained by the dilution effect and the occurrence of a small swelling peak after about 1 day. This swelling peak was already observed for cement paste mixes and was attributed to the formation of ettringite [15]. A lower autogenous shrinkage for concrete mixtures with fly ash was already reported by other researchers [32–36] and was attributed to the low reactivity of fly ash, the inhibited hydration reaction at early age and the dilution effect [33,34]. Bouhamou et al. [11] also reported lower autogenous deformations for a concrete mix with addition of calcined mud.

3.4. Total shrinkage

The average results of the total shrinkage strains are shown in Fig. 9 (negative values correspond to shrinkage). The total shrinkage was only measured for the two CFC mixes with the highest replacement ratio (CFC 30 and CFC 40), in which the highest impact of CFC was expected. Also for the total shrinkage, lower values are observed for the CFC blended cement mixes. This can be explained by the dilution effect, the reduced hydration rate and the altered porosity of the CFC blended cement concretes. The RC II mix follows the same trend as the CFC blended cement mixes at early ages. However, from about 7 days the total shrinkage of the RC II mix starts to increase more, and reaches about the same values as the RC I mix. A decrease in total shrinkage was also observed for concrete with addition of calcined mud [11]. However, for concrete mixes with fly ash, both a decrease and increase in total shrinkage are reported in literature [24,32–34,37].

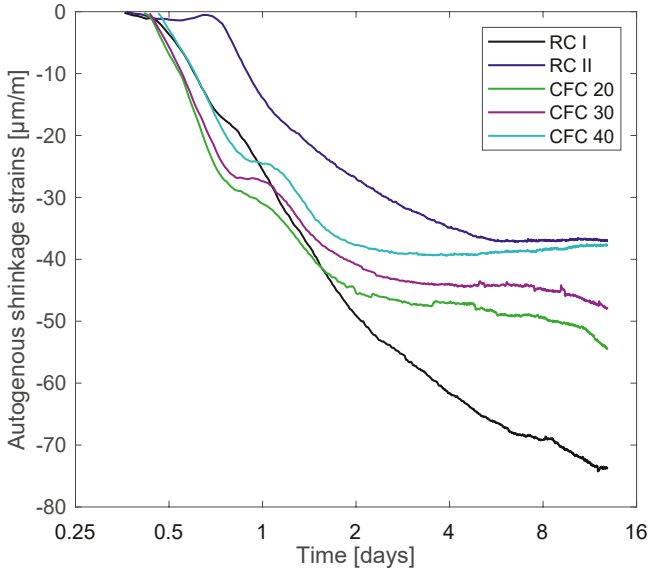

Fig. 8. Autogenous shrinkage development of the different concrete mixes up to 14 days.

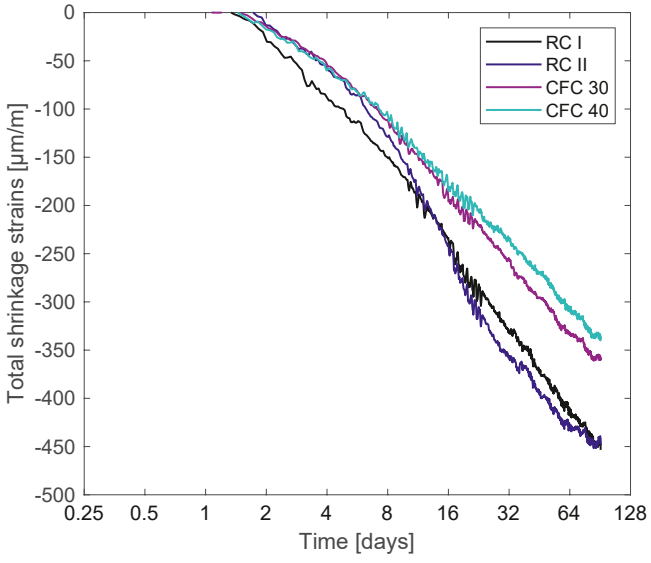

Fig. 9. Total shrinkage development of the different concrete mixes up to 90 days.

4. Modelling

4.1. Temperature development

Model. In order to determine the evolution of temperature (T) inside a concrete element, the energy balance equation, which includes the heat release due to the hydration reaction, is solved [38–40]:

$$C \cdot \dot{T} = \nabla \cdot (k \cdot \nabla T) + \dot{Q} \tag{4}$$

where C is the volumetric heat capacity [J/m^3/K], k is the thermal conductivity [W/m/K] and Q is the cumulative heat release [J/m^3]. Since the volumetric heat capacity and thermal conductivity can be considered as constant in space and time, the heat equation can be expressed as:

$$C \cdot \dot{T} = k \cdot \Delta T + \dot{Q} \tag{5}$$

The heat source term ($\dot{Q}$) comes from the exothermic hydration reaction and can be expressed as:

$$\dot{Q} = L \cdot \dot{\xi} \tag{6}$$

where L is the latent heat of hydration [J/m^3] and $\dot{\xi}$ is the rate of degree of hydration [−]. Since the hydration of cement paste is a thermo-activated process, the evolution of the degree of hydration can be obtained by using an Arrhenius type law [41]:

$$\dot{\xi} = \tilde{A}(\xi) \cdot \exp\left(\frac{E_a}{R} \cdot \left(\frac{1}{293} - \frac{1}{T}\right)\right) \tag{7}$$

where E_a is the activation energy [J/mol], R is the ideal gas constant [8.314 J/mol/K] and $\tilde{A}(\xi)$ is the chemical affinity [1/h].

The boundary conditions for early-age concrete are assumed to be of the convective type. Convection refers to the heat transfer occurring between the concrete surface and the surrounding air [38,42]. The imposed heat flux (φ) equals:

$$\varphi = h \cdot (T_S - T_{ext}) \cdot \mathbf{n} \tag{8}$$

where h is the coefficient of heat exchange by convection [W/m^2/K], T_S is the surface temperature [K], T_{ext} is the ambient temperature [K] and **n** is the normal unit vector to the surface.

Parameter identification. The latent heat of hydration L and the chemical affinity $\tilde{A}(\xi)$ can be obtained experimentally from isothermal calorimetry results. The determination of these parameters mainly consists of extrapolating the laboratory test results, by fitting mathematical models to the experimental observations. The development of the cumulative heat Q (and the hydration in general) in time can be best represented by an exponential/S-shaped mathematical model:

$$Q(t) = Q_\infty \cdot \exp\left(-\frac{\tau}{t}\right)^\beta \tag{9}$$

where Q_∞ is the ultimate cumulative heat (equal to the latent heat of hydration L), τ is the hydration time parameter and β is the hydration shape parameter (all fitting parameters).

The normalised affinity $\tilde{A}(\xi)$ characterises the macroscopic hydration kinetics for a given concrete mixture and is associated with the micro-diffusion process of water reacting with unhydrated cement [39,43]. The chemical affinity $\tilde{A}(\xi)$ can be calculated from the experimental data using the following equation:

$$\tilde{A}(\xi) = \frac{\dot{Q}}{L} \cdot \exp^{-1}\left(\frac{E_a}{R} \cdot \left(\frac{1}{293} - \frac{1}{T}\right)\right) \tag{10}$$

and several models could be used to describe this process. Cervera et al. [43] developed the following analytical form:

$$\tilde{A}(\xi) = \frac{k_\xi}{\eta_{\xi 0}} \cdot \left(\frac{A_{\xi 0}}{k_\xi \cdot \xi_\infty} + \xi\right) \cdot (\xi_\infty - \xi) \cdot \exp\left(-\bar{\eta} \cdot \frac{\xi}{\xi_\infty}\right) \tag{11}$$

where ξ_∞ is the final degree of hydration and k_ξ, $A_{\xi 0}$, $\eta_{\xi 0}$ and $\bar{\eta}$ are material constants. In order to reduce the amount of parameters, the following equation will be used to describe the chemical affinity:

$$\tilde{A}(\xi) = \beta \cdot \left(1 + \frac{\xi}{\xi_1}\right) \cdot \left(1 - \frac{\xi}{\xi_\infty}\right) \cdot \exp\left(-\bar{\eta} \cdot \frac{\xi}{\xi_\infty}\right) \tag{12}$$

where $\beta = \frac{A_{\xi 0}}{\eta_{\xi 0}}$, $\xi_1 = \frac{A_{\xi 0}}{k_\xi \cdot \xi_\infty}$, $\bar{\eta}$ (and ξ_∞) are then considered as the fitting parameters.

Results. The results of the modelled cumulative heat are shown in Fig. 10, compared to the experimental results. It is observed that the development of the modelled cumulative heat corresponds well to the development of the experimental data.

The temperature development of the different concrete compositions as a function of time and distance from the center of the specimen is shown in Fig. 11, assuming the boundary conditions summarized in Table 3. The thickness of the specimen is chosen as 1.2 m, representing a massive structure. The maximal temperature developed in the structure is also shown on the graphs in Fig. 11. The model indicates that the RC I concrete mix reaches the highest maximal temperature, while the blended cement mixes show lower maximal temperatures. This can be explained by the lower cumulative heat of the blended cement mixes, compared to the RC I reference mix. The temperature difference between the three CFC blended cement mixes is negligible.

4.2. Mechanical properties development

Model. According to Eurocode 2 (2010) [17], the development of the studied mechanical properties in time can be described by the following equations:

$$X(t_{eq}) = X_{28} \cdot \beta_X(t_{eq})^{n_X} \tag{13}$$

$$\beta_X = \exp\left[s \cdot \left(1 - \sqrt{\frac{28 - t_0}{t_{eq} - t_0}}\right)\right] \tag{14}$$

where X is the studied mechanical material property, X_{28} is the value of the material property after 28 days, β_X is a function describing the

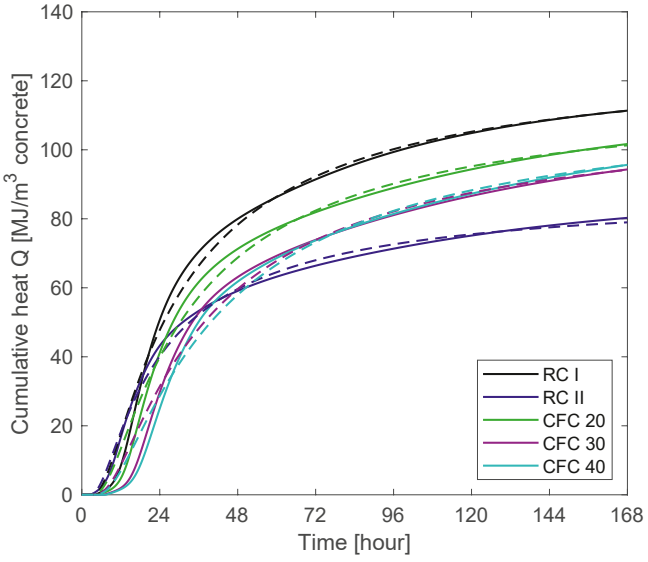

Fig. 10. Cumulative heat of the different concrete mixes: comparison between the experiments (full lines) and model (dashed lines).

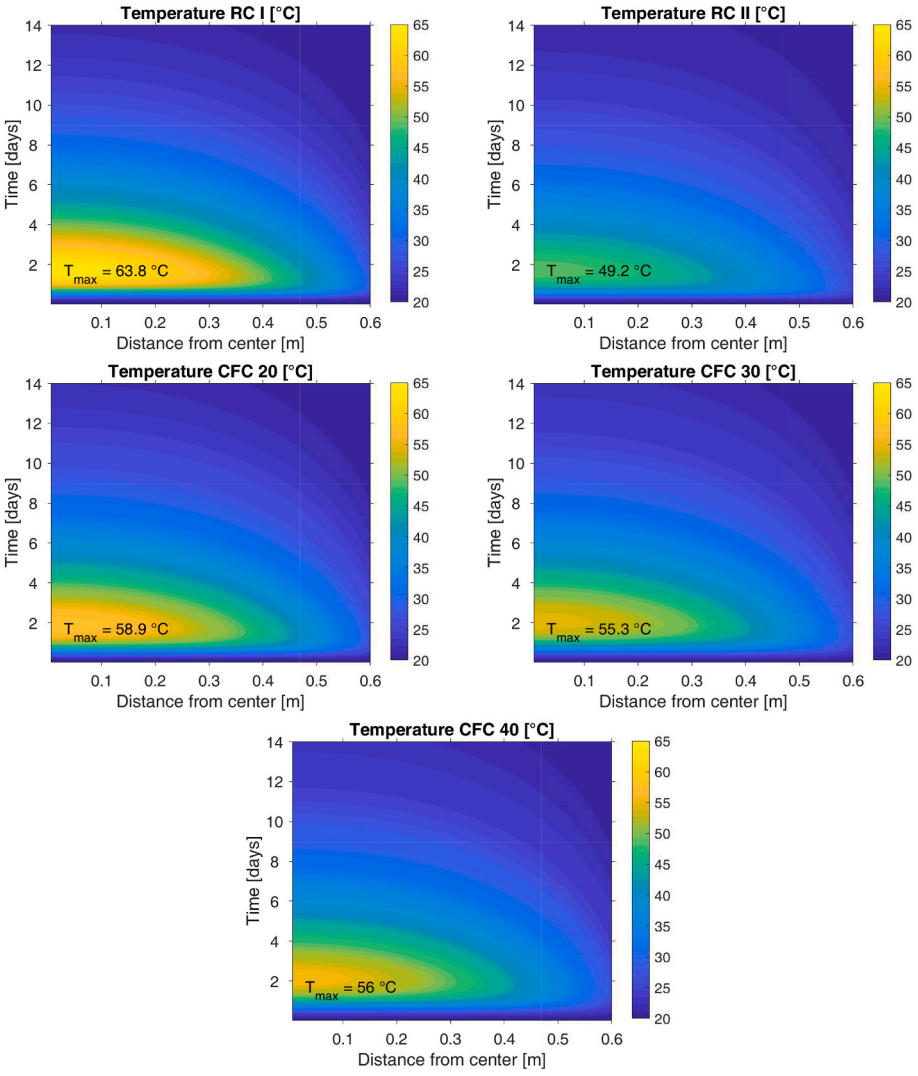

Fig. 11. Temperature development of the different concrete mixes as a function of time and distance from the center of the specimen.

Table 3
Boundary conditions and thickness used to solve the heat equation.

Initial temperature T_0	20 °C
External temperature T_{ext}	20 °C
Convection coefficient h	17.5 W/m^2/K
Thickness e	1.2 m

development of the material property in time, n_X is an aging parameter, s is a coefficient depending on the type of cement, t_0 is the final setting time and t_{eq} is the equivalent time, which can be derived from the temperature development as:

$$t_{eq} = \sum_{0}^{t} \exp\left(\frac{E_a}{R} \cdot \left(\frac{1}{293} - \frac{1}{T}\right)\right) \cdot \Delta t \tag{15}$$

with t the age of the concrete.

For the compressive strength (f_c), tensile strength (f_{ct}), and static Young's modulus (E_c), the equations become:

$$f_c(t_{eq}) = f_{c28} \cdot \exp\left[s \cdot \left(1 - \sqrt{\frac{28 - t_0}{t_{eq} - t_0}}\right)\right]^{n_{f_c}} \tag{16}$$

$$f_{ct}(t_{eq}) = f_{ct28} \cdot \exp\left[s \cdot \left(1 - \sqrt{\frac{28 - t_0}{t_{eq} - t_0}}\right)\right]^{n_{f_{ct}}} \tag{17}$$

$$E_c(t_{eq}) = E_{c28} \cdot \exp\left[s \cdot \left(1 - \sqrt{\frac{28 - t_0}{t_{eq} - t_0}}\right)\right]^{n_{E_c}} \tag{18}$$

Parameter identification. Since the coefficient s is a cement type dependent parameter, it is constant for all three material properties. According to Eurocode 2 [17], the value of s should be equal to 0.20 for class R cement (and CEM 52.5 N), 0.25 for class N cement (and CEM 32.5R) and 0.38 for class S cement (and CEM 32.5 N). However, Kanstad et al. [44] found values of 0.12–0.22 for blended cements, Darquennes and Benboudjema [45] found values of 0.09–0.23 for alkali activated blended cements and Klemczak et al. [46] found values of 0.20–0.38 for cements with mineral additives. This demonstrates the importance of experimental data to accurately determine the coefficient s, especially for (new) blended cement systems. The experimental results of the compressive strength were used here to determine this coefficient s, for multiple reasons: compressive strength tests were performed at six different points of time (while tensile strength and static Young's modulus test were only performed at three different points of time), the compressive strength test is a direct test and is easy to perform, and the experimental error and statistical scatter of the compressive strength

results were smallest.

In literature, only one value for n_{fc} is found: 1 [17,18,44]. In order to validate this value for blended cement concretes, model fitting was done both with taking n_{fc} equal to 1 and with taking n_{fc} as a fitting parameter. Since experimental data of the compressive strength after 28 days is available, parameter f_{c28} can be taken, or as the experimentally determined value, or as a fitting parameter. Both options were considered. The above described methodology leads to four different 'fitting' methods in order to validate the Eurocode 2 model (Eq. (13) and (14)) for new blended cement systems, summarized in Table 4. The resulting parameters of the model fitting can be found in Table 5. It was chosen to only consider one parameter s and one parameter n_{f_c} for the three CFC blended cement systems, since these parameters are cement/binder type dependent parameters and in this way, one general/uniform value is valid for all CFC mixes.

It can be seen from Table 5 that the values of s are lower than the values predicted by Eurocode 2 [17] for cement with normal strength development. However, they are in the range of the values found by Kanstad [44] for blended cements. Compared to the OPC reference mix (RC I), the values of s are higher for the blended cement mixes, demonstrating a slower mechanical properties development of the blended cement mixes. In order to compare the four different fitting methods, an average root mean square error (RMSE) is calculated per method. The RMSE of the different methods is also shown in Table 5 and is calculated as:

$$\mathrm{RMSE} = \sqrt{\frac{\sum_i \left(\hat{y}_i - y_i\right)^2}{n}} \tag{19}$$

with $\hat{y}_i$ the modelled values of the compressive strength, y_i the experimental values of the compressive strength and n the amount of data points. Remarkable is the fact that the RMSE's of methods A & C and B & D are exactly the same. This proves that the results of fitting methods C and D are not unique and that both methods do not contribute to a better fitting. Comparing the errors of method A and B, method B shows a slightly lower RMSE, resulting in a slightly better fit. However, since the difference in RMSE is very small and in order to keep the amount of fitting parameters as low as possible, it is chosen to retain the values of method A. The Eurocode 2 model for describing the compressive strength development, is thus proven to be also valid for new blended cement mixtures, provided that parameter s is adjusted according to the new blended cement system.

Since the values of the aging parameters n_{fct} and n_{Ec} vary considerably in literature (from 0.5 to 1 for n_{fct} and from 0.3 to 0.5 for n_{Ec} [17,18,44]), these values are taken as fitting parameters. Since the tensile strength and static E-modulus were not determined experimentally after 28 days, the parameters f_{ct28} and E_{c28} were also considered as fitting parameters. The results of the model fitting can be found in Table 6. The values of n_{fct} are in the range of the values found in literature, while the values of n_{Ec} were lower than the ones predicted by literature, meaning that the development of the static E-modulus is faster than in literature.

Results. In Figs. 12–14 the development of the considered mechanical properties according to Eurocode 2 is plotted. For the compressive strength, the RC I mix reaches the highest values during early ages. From the age of 4.5 days approximately, the compressive strength of the CFC 20 mix surpass the compressive strength of the RC I mix and later on, also the compressive strength of CFC 30 and CFC 40 overtake the compressive strength values of RC I. After approximately 14 days, the values of the compressive strength of all CFC blended cement mixes thus surpass the RC I compressive strength values. The values of the compressive strength of the RC II mix with fly ash are remarkable lower. Regarding the tensile strength, on the other hand, the RC I mix always reaches the highest values, followed by the CFC mixes and the RC II mix. The static elastic modulus of the CFC 20 mix reaches the highest values, while there is a gradually decrease of the final static elastic modulus values for increasing replacement of CFC.

In Figs. 15–17, the relative values of the mechanical properties are plotted. The curves of all CFC mixes overlap, since the same cement type dependent parameter s and the same aging parameters n are used. In contrast to the absolute values of the compressive strength, the RC I mix reaches the highest relative values, so the strength development is the fastest, while the development of the blended cement mixes is relatively slower. It is also observed that the compressive strength development of the CFC mixes is slightly slower than the development of the RC II mix with fly ash. So although the CFC mixes reach the highest absolute compressive strength values (see Fig. 12), the development of their strength is slower compared to the two reference mixes. This was already visible in the higher value of s for the CFC blended cement mixes (see Table 6), compared to the two reference mixes. For both the tensile strength and static elastic modulus, the same behaviour is observed. The RC I and RC II mixes show the fastest development of the mechanical properties, while the CFC blended cement concretes show a slower development. This behaviour is known for blended cement concretes and can be explained by the pozzolanic reaction, taking place much later than the hydration reactions, slowing down the strength development.

Table 4
Different methods for model fitting of the compressive strength results according to Eq. (16).

	s	n_{fc}	f_{c28}
Method A	fitting parameter	1	f_{cm28}
Method B	fitting parameter	1	fitting parameter
Method C	fitting parameter	fitting parameter	f_{cm28}
Method D	fitting parameter	fitting parameter	fitting parameter

4.3. Shrinkage development

Empirical shrinkage models generally describe shrinkage as the product of two terms: the final/ultimate shrinkage ε_∞ (a magnitude function) and the shrinkage rate β or S (a time function). For autogenous shrinkage, the general equation is:

$$\varepsilon_{au}(t) = \varepsilon_{au\infty} \cdot \beta(t) \tag{20}$$

where $\varepsilon_{au\infty}$ is the ultimate autogenous shrinkage, depending on the concrete mix design and mechanical properties, and $\beta(t)$ is the autogenous rate function. For drying shrinkage, the general equation is:

$$\varepsilon_{dr}(t) = \varepsilon_{dr\infty}(\mathrm{RH}, T) \cdot S(t, t_s, h_0) \tag{21}$$

where $\varepsilon_{dr\infty}(\mathrm{RH}, T)$, the ultimate drying shrinkage, depends both on the concrete mix design and mechanical properties, as well as on the initial and external conditions: temperature (T) and relative humidity (RH). The rate function $S(t, t_s, h_0)$ depends on the age of the concrete (t), the age of the concrete at the start of drying (t_s) and the notional size of the specimen (h_0), defined as:

$$h_0 = \frac{2 \cdot V}{S} \tag{22}$$

where V is the volume and S the drying surface of the specimen. In this case the notional size is taken as D/2 (with D the diameter of the specimen), neglecting drying at the top and bottom of the specimen. This assumption is acceptable, since the ratio of the height of the specimen to the diameter of the specimen, is relatively high (i.e. 2.5).

4.3.1. Autogenous shrinkage

For autogenous shrinkage, five different existing models are considered: the Bazant B4 model [22], the Eurocode 2 model [17], the Model Code 2010 model [18], the β-n model (see Eq. (13) and (14)) and a model described by Rifai [47]. The expressions of the different autogenous shrinkage models, in function of the equivalent time (t_{eq}),

Table 5
Parameters of the compressive strength development according to Eq. (16), using four different fitting methodologies (see Table 4). The values in *italic* are fitting parameters. f_{c28} in MPa.

	Method A			Method B			Method C			Method D		
	s	n_{fc}	f_{c28}	*s*	n_{fc}	f_{c28}	*s*	n_{fc}	f_{c28}	*s*	n_{fc}	f_{c28}
RC I	*0.14*	1	62.28	*0.15*	1	*64.30*	*0.15*	*0.97*	62.28	*0.17*	*0.90*	*64.30*
RC II	*0.20*	1	47.16	*0.21*	1	*47.88*	*0.21*	*0.97*	47.16	*0.22*	*0.95*	*47.88*
CFC 20	*0.23*	1	71.72	*0.22*	1	*69.18*	*0.24*	*0.96*	71.72	*0.24*	*0.94*	*69.18*
CFC 30	*0.23*	1	65.97	*0.22*	1	*67.43*	*0.24*	*0.96*	65.97	*0.24*	*0.94*	*67.43*
CFC 40	*0.23*	1	64.76	*0.22*	1	*63.74*	*0.24*	*0.96*	64.76	*0.24*	*0.94*	*63.68*
RMSE	2.28 MPa			1.97 MPa			2.28 MPa			1.97 MPa		

Table 6
Parameters of the tensile strength and static E-modulus development according to Eq.(17) and (18).

	s	n_{fct}	f_{ct28}	n_{Ec}	E_{c28}
RC I	0.14	0.97	3.38	0.29	34.00
RC II	0.20	0.61	2.35	0.20	31.51
CFC 20	0.23	0.65	3.04	0.23	36.22
CFC 30	0.23	0.65	2.75	0.23	33.96
CFC 40	0.23	0.65	2.83	0.23	31.80

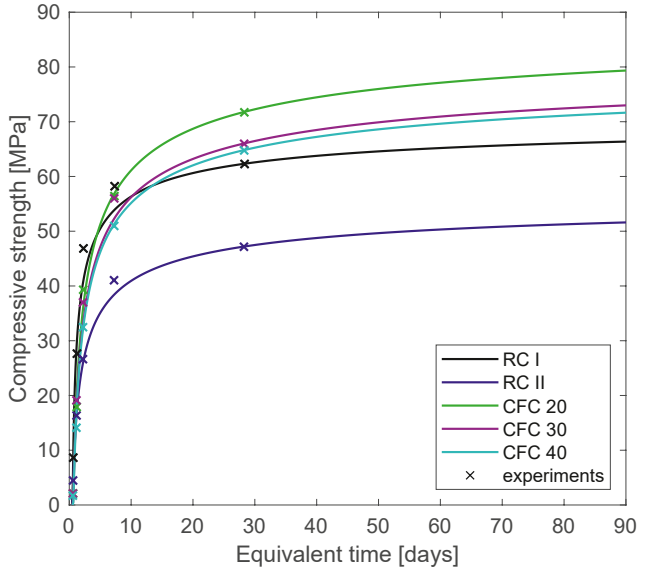

Fig. 12. Compressive strength model of the different concrete compositions, compared to the experimental data.

are summarized below. The autogenous shrinkage only starts to develop from the moment of final setting (t_0).

- Bazant B4 model

$$\varepsilon_{au}(t_{eq}) = \varepsilon_{au\infty} \cdot \left[1 + \left(\frac{\tau_{au}}{t_{eq} - t_0}\right)^{\alpha}\right]^{r_t} \quad (23)$$

where $\varepsilon_{au\infty}$ (the final autogenous shrinkage), τ_{au} (the autogenous shrinkage halftime), α and r_t are cement type dependent parameters, determined by fitting the experimental results to the model [22].

- Eurocode 2 model (EC 2 model)

$$\varepsilon_{au}(t_{eq}) = \varepsilon_{au}(\infty) \cdot \beta_{au}(t_{eq}) \quad (24)$$

with $\varepsilon_{au}(\infty)$ the final autogenous shrinkage and $\beta_{au}(t_{eq})$ the time function, described as:

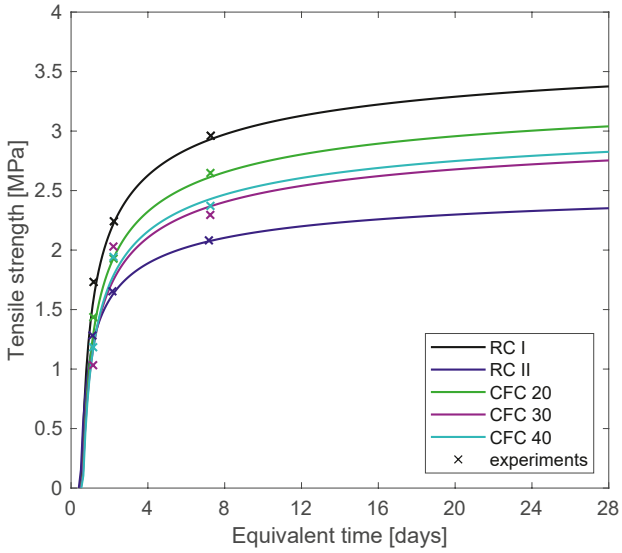

Fig. 13. Tensile strength model of the different concrete compositions, compared to the experimental data.

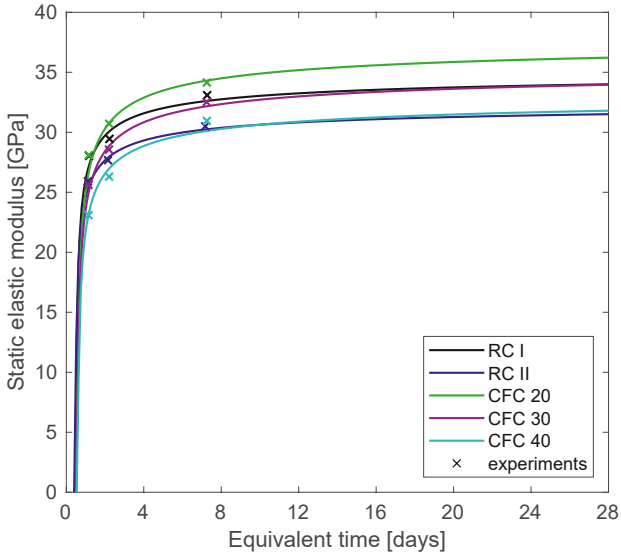

Fig. 14. Static E-modulus model of the different concrete compositions, compared to the experimental data.

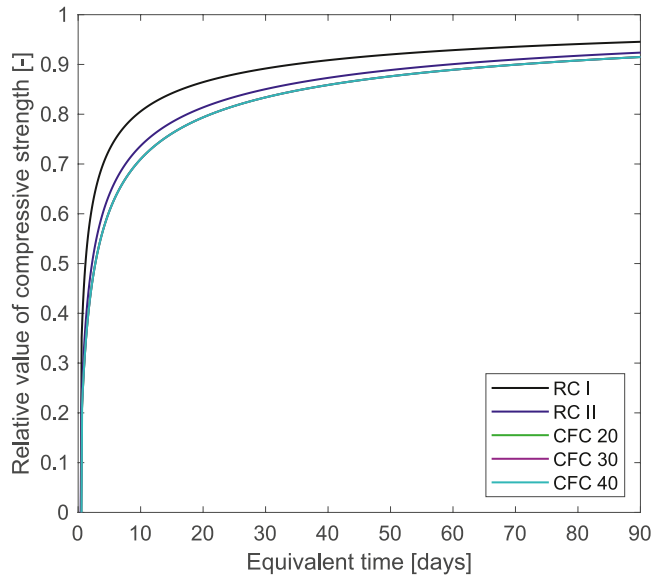

Fig. 15. Relative compressive strength development of the different concrete mixes.

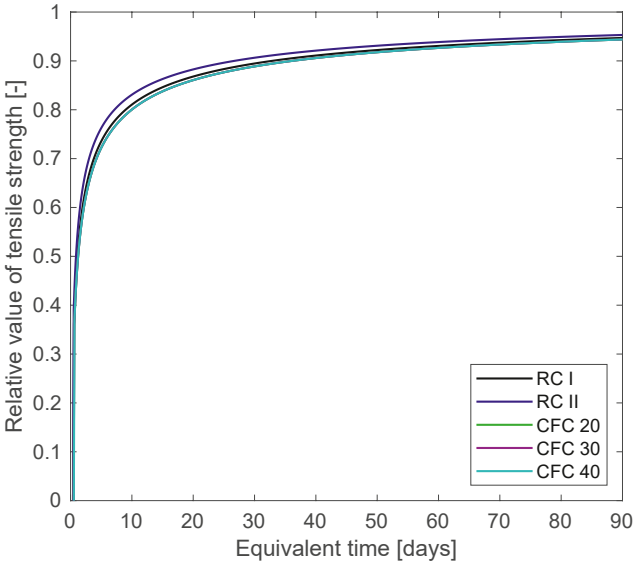

Fig. 16. Relative tensile strength development of the different concrete mixes.

$$\varepsilon_{au}(\infty) = 2.5 \cdot (f_{ck} - 10) \cdot 10^{-6} \tag{25}$$

$$\beta_{au}(t_{eq}) = 1 - \exp\left(-0.2 \cdot \sqrt{t_{eq} - t_0}\right) \tag{26}$$

with f_{ck} the characteristic compressive strength of the concrete [17].

- Model Code 2010 model (MC 2010 model)

$$\varepsilon_{au}(t_{eq}) = \varepsilon_{au,0}(f_{cm}) \cdot \beta_{au}(t_{eq}) \tag{27}$$

with $\varepsilon_{au,0}(f_{cm})$ the notional autogenous shrinkage coefficient and $\beta_{au}(t_{eq})$ the time function, described as:

$$\varepsilon_{au,0}(f_{cm}) = -\alpha_{au} \cdot \left(\frac{f_{cm}}{60 + f_{cm}}\right)^{2.5} \cdot 10^{-6} \tag{28}$$

$$\beta_{au}(t_{eq}) = 1 - \exp\left(-0.2 \cdot \sqrt{t_{eq} - t_0}\right) \tag{29}$$

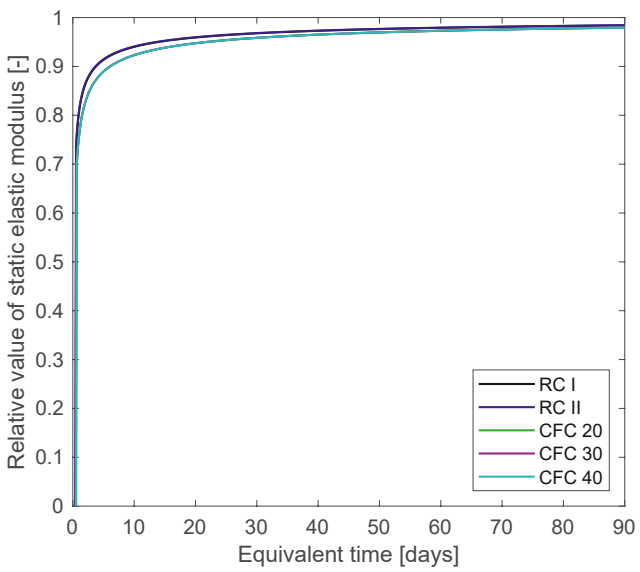

Fig. 17. Relative static E-modulus development of the different concrete mixes.

with α_{au} a cement type dependent parameter, considered here as a fitting parameter, and f_{cm} the mean concrete compressive strength [18].

- β-n model

$$\varepsilon_{au}(t_{eq}) = \varepsilon_{au,28} \cdot \beta_{\varepsilon_{au}}(t_{eq})^{n_{\varepsilon au}} \tag{30}$$

with $\varepsilon_{au,28}$ the autogenous shrinkage value after 28 days and $n_{\varepsilon au}$ an aging parameter, both considered as fitting parameters. $\beta_{\varepsilon_{au}}(t_{eq})$ is the time function, described as:

$$\beta_{\varepsilon_{au}}(t_{eq}) = \exp\left[s \cdot \left(1 - \sqrt{\frac{28 - t_0}{t_{eq} - t_0}}\right)\right] \tag{31}$$

with s a cement type dependent parameter, already determined for every concrete composition in 4.2.

- Rifai model

$$\varepsilon_{au}(t_{eq}) = y_0 + A_1 \cdot \exp\left(-\frac{t_{eq} - t_0}{t_1}\right) + A_2 \cdot \exp\left(-\frac{t_{eq} - t_0}{t_2}\right) \tag{32}$$

with y_0, A_1, A_2, t_1 and t_2 all fitting parameters [47].

It should be noted that for the Bazant B4 model, a simplified model from Ref. [22] is used. Parameters $\varepsilon_{au\infty}$, τ_{au}, α and r_t are directly considered as cement type dependent fitting parameters, rather than calculating them from an even larger set of cement type dependent parameters. It should also be remarked that all models, except for the Eurocode 2 model, depend on one or more cement type depending parameters, which are all considered as fitting parameters. The amount of fitting parameters strongly determines the goodness of fit. The Eurocode 2 model does not depend on the cement type, only on the compressive strength of the concrete mix. Furthermore, the Rifai model does not follow the general mathematical formula for autogenous shrinkage development (see Eq. (20)), but uses a different formulation. Finally, all cement type dependent fitting parameters of the CFC mixes are (as also with the cement type dependent mechanical properties parameters) taken as constant, in order to get general/uniform cement type dependent parameters for all CFC mixes.

The results of the model fitting are presented in Fig. 18. At first sight, it is remarkable that the Eurocode 2 model and Model Code 2010 model deviate the most from the experimental results, both at very early ages, as well as at later ages. Since the same time functions β were used for

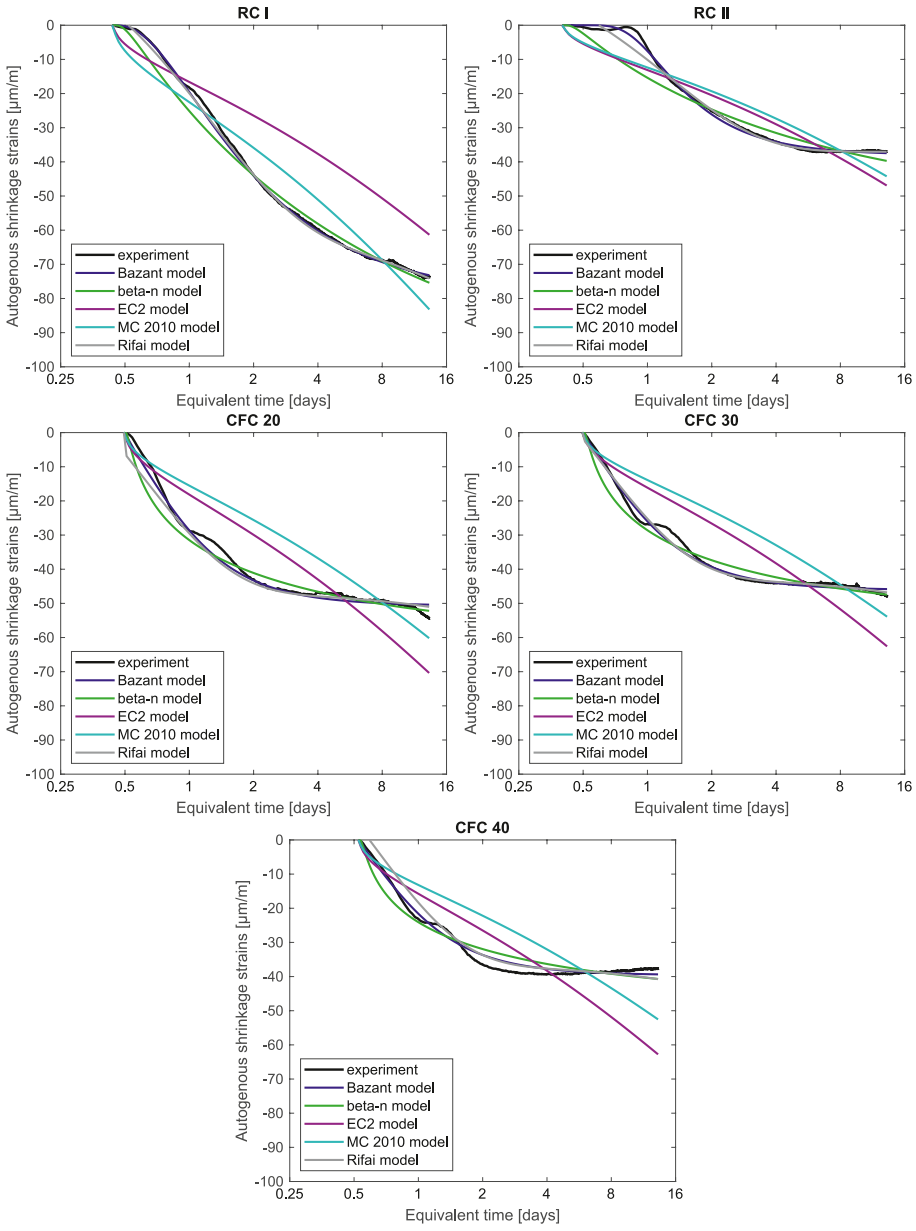

Fig. 18. Different autogenous shrinkage models for the different concrete mixes, compared with the experimental results.

both models, the models follow the same shrinkage development, slightly differing due to a different final autogenous shrinkage value. The other three models (Bazant model, β-n model and Rifai model) all predict the autogenous shrinkage quite well. The small autogenous swelling which is observed for the CFC mixes, however, cannot be taken into account in the different models. At early ages all models therefore over- or underestimate the real autogenous shrinkage.

In order to compare the different models and determine the best predictor, a root mean square error (RMSE) is determined. The RMSE of the different autogenous shrinkage models for the different concrete compositions is shown in Fig. 19. As already noticed in Fig. 18, the EC 2 and MC 2010 models show the biggest error. The difference in error between the other three models is quite small. The small errors of the Bazant model and the Rifai model are quite obvious, since for these models, respectively 4 and 5 fitting parameters were considered. Overall, the Bazant B4 model can be considered as the best predictor for autogenous shrinkage, both for the traditional concrete mix as for the blended cement mixtures.

4.3.2. *Drying/total shrinkage*

For drying shrinkage, four different existing models are considered: the Bazant B4 model [22], the Eurocode 2 model [17], the Model Code 2010 model [18] and the β-n model. The expressions of the different drying models are summarized below.

- Bazant B4 model

$$\varepsilon_{dr}\left(\tilde{t},\tilde{t}_s\right)=\varepsilon_{droo}\left(\tilde{t}_s\right)\cdot k_h\cdot S\left(\tilde{t}\right) \tag{33}$$

where $\tilde{t}_s$ is the temperature corrected age at start of drying ($t_{s,eq}$) and $\tilde{t}$ is the temperature corrected duration of drying ($t_{eq}-t_{s,eq}$). The humidity dependent correction factor kh and the time curve $S(\tilde{t})$ are respectively given by:

$$k_h=\begin{cases}1-h^3 & h\le 0.98\\ 12.94\cdot(1-h)-0.2 & 0.98\le h\le 1\end{cases} \tag{34}$$

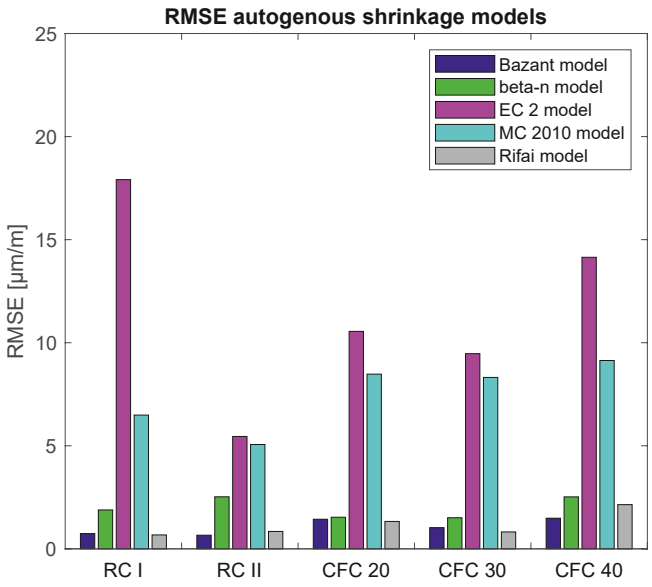

Fig. 19. RMSE of the different autogenous shrinkage models for the different concrete compositions.

$$S(\tilde{t}) = \tanh\sqrt{\frac{\tilde{t}}{\tau_{dr}}} \tag{35}$$

with h the ambient relative humidity and τ_{dr} the drying shrinkage halftime, which is:

$$\tau_{dr} = \tau_0 \cdot k_{\tau a} \cdot (k_s \cdot h_0)^2 \tag{36}$$

with τ_0 a cement type dependent parameter, $k_{\tau a}$ an aggregate dependent parameter, k_s a parameter depending on the geometry of the specimen and h_0 the notional size or effective thickness of the specimen. The final drying shrinkage ($\varepsilon_{dr\infty}$) and the parameter τ_0 are cement type dependent parameters, determined by fitting the experimental results to the model.

- Eurocode 2 model

$$\varepsilon_{dr}(t_{eq}) = k_h \cdot \varepsilon_{dr,0} \cdot \beta_{dr}(t_{eq}, t_s) \tag{37}$$

with k_h a coefficient depending on the effective thickness (h_0), $\varepsilon_{dr,0}$ the nominal unrestrained drying shrinkage value and $\beta_{dr}(t_{eq}, t_s)$ the time function, respectively described as:

$$\varepsilon_{dr,0} = 0.85 \cdot \left[(220 + 110 \cdot \alpha_{dr1}) \cdot \exp\left(-\alpha_{dr2} \cdot \frac{f_{cm}}{f_{cm0}}\right)\right] \cdot 10^{-6} \cdot \beta_{RH} \tag{38}$$

$$\beta_{dr}(t_{eq}, t_s) = \frac{(t_{eq} - t_s)}{(t_{eq} - t_s) + 0.04 \cdot \sqrt{h_0^3}} \tag{39}$$

with α_{dr1} and α_{dr2} coefficients depending on the type of cement, here considered as fitting parameters, f_{cm} the mean concrete compressive strength, f_{cm0} equal to 10 MPa and β_{RH} a relative humidity dependent coefficient, described as:

$$\beta_{RH} = 1.55 \cdot \left[1 - \left(\frac{RH}{RH_0}\right)^3\right] \tag{40}$$

with RH the ambient relative humidity and RH_0 equal to 100%.

- Model Code 2010 model

$$\varepsilon_{dr}(t_{eq}) = \varepsilon_{dr,0}(f_{cm}) \cdot \beta_{RH}(RH) \cdot \beta_{dr}(t_{eq}, t_s) \tag{41}$$

with $\varepsilon_{dr,0}(f_{cm})$ the notional drying shrinkage coefficient, $\beta_{RH}(RH)$ a coefficient taking into account the effect of the ambient relative humidity and $\beta_{dr}(t_{eq}, t_s)$ a time function, respectively described as:

$$\varepsilon_{dr,0}(f_{cm}) = [(220 + 110 \cdot \alpha_{dr1}) \cdot \exp(-\alpha_{dr2} \cdot f_{cm})] \cdot 10^{-6} \tag{42}$$

$$\beta_{RH}(RH) = \begin{cases} \\ -1.55 \cdot \left[1 - \left(\frac{RH}{100}\right)^3\right] 40 \le RH < 99 \cdot \beta_{s1} \; 0.25RH \ge 99 \cdot \beta_{s1} \end{cases} \tag{43}$$

$$\beta_{dr}(t_{eq}, t_s) = \sqrt{\frac{(t_{eq} - t_s)}{(t_{eq} - t_s) + 0.035 \cdot h_0^2}} \tag{44}$$

with α_{dr1} and α_{dr2} coefficients depending on the type of cement, here considered as fitting parameters, f_{cm} the mean concrete compressive strength, RH the ambient relative humidity and β_{s1} equal to $(35/f_{cm})^{0.1}$.

- β-n model

$$\varepsilon_{dr}(t_{eq}) = \varepsilon_{dr,28} \cdot \beta_{\varepsilon_{dr}}(t_{eq})^{n_{\varepsilon_{dr}}} \tag{45}$$

with $\varepsilon_{dr,28}$ the drying shrinkage value after 28 days and $n_{\varepsilon au}$ an aging parameter, both considered as fitting parameters. $\beta_{\varepsilon_{au}}$ is the time function, described as:

$$\beta_{\varepsilon_{dr}} = \exp\left[s \cdot \left(1 - \sqrt{\frac{28 - t_s}{t_{eq} - t_s}}\right)\right] \tag{46}$$

with s a cement type dependent parameter, already determined in 4.2.

All drying shrinkage models, except for the β-n model, are depending both on the effective/notional size (h_0) and on the ambient relative humidity (RH). It should also be remarked that only the Eurocode 2 and Model Code 2010 models depend on the compressive strength of the concrete mix. Furthermore, all models have the same amount of cement type dependent parameters and thus the same amount of fitting parameters. Also here, these parameters are taken constant for all CFC mixes.

The measured total shrinkage strains are the sum of the drying and autogenous shrinkage strains. The above described models for drying shrinkage thus only apply for a part of the measured deformations. In order to also take the autogenous deformations into account, the total shrinkage results are modelled as the sum of the autogenous shrinkage strains and the drying shrinkage strains, using the previously found parameters for the autogenous shrinkage models. The results of the combined model fitting are presented in Fig. 20 and the RMSE of the different models is shown in Fig. 21. What stands out immediately is the fact that the total shrinkage model curves do not all start at the same point. This is due to the fact that the previous autogenous shrinkage models are taken into account, and at the moment of start of drying, already some autogenous shrinkage has developed. In general, all four models show a quite good fit, especially at later ages. During the very early ages, the Eurocode 2 and β-n model show a better fit, compared to the Bazant B4 and the Model Code 2010 model. This is mainly the result of the different descriptions of the time functions for the different models. At later ages, all models show a quite perfect fit for the RC I mix, while for the blended cement concretes, the Bazant B4 and β-n model show a better fit. Looking at the errors in Fig. 21, it can be seen that there is no clear trend between the errors of the different models for the different concrete mixes. For the RC I and RC II mixes, the Bazant B4 and the MC 2010 models show the worst fit, while for the CFC blended cement mixes, the EC 2 and MC 2010 models show the worst fit. Overall, the β-n model appears to be the best predictor for all compositions, followed by the Eurocode 2 model for the two reference mixes and the Bazant B4 model for the two CFC mixes.

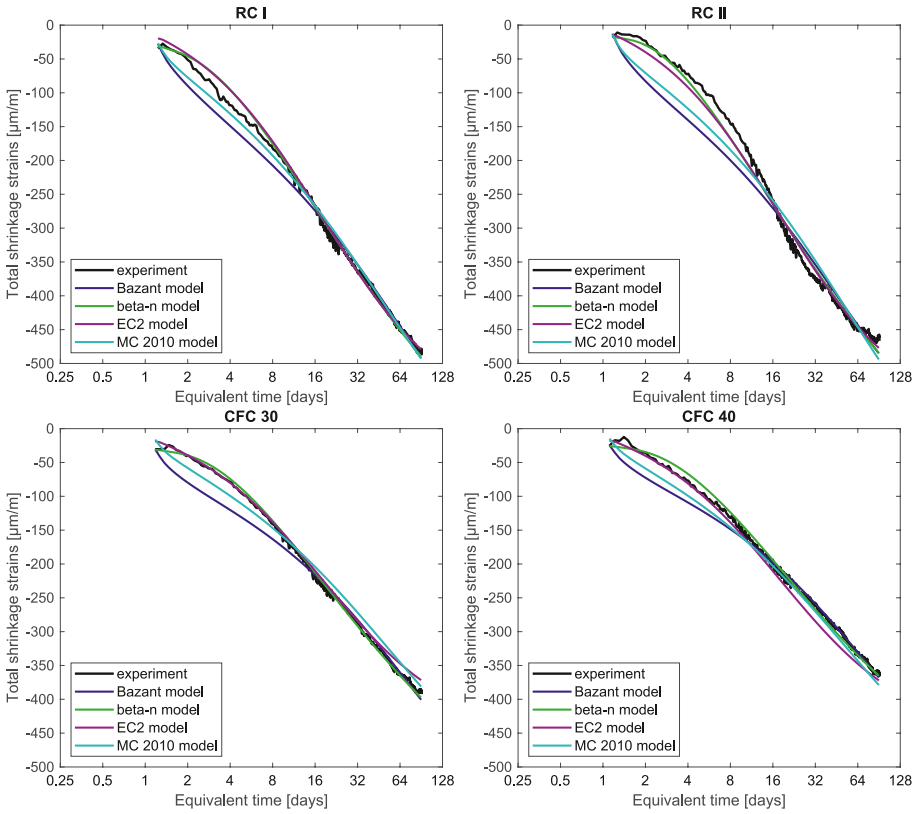

Fig. 20. Different total shrinkage models for the different concrete mixes, compared with the experimental results.

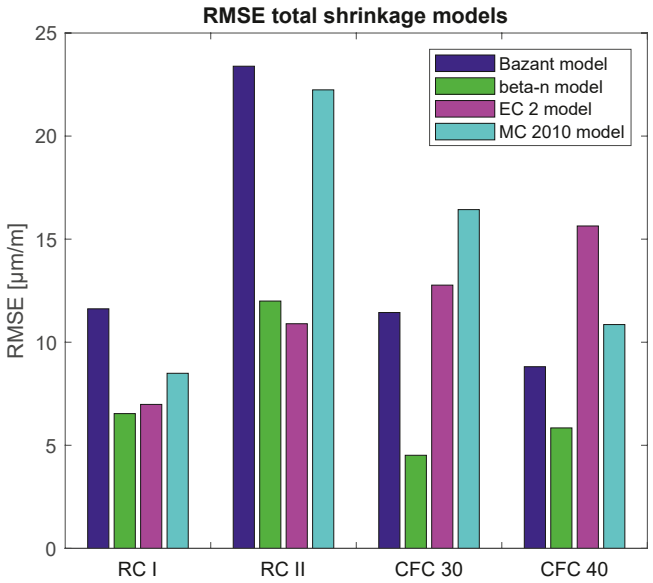

Fig. 21. RMSE of the different total shrinkage models for the different concrete compositions.

The previously used methodology, however, is not completely correct, since the autogenous deformations occurring in completely sealed (autogenous) conditions, are not equal to the autogenous deformations occurring in a drying environment. In drying conditions, less water is available, so the hydration will be slowed down and will be less complete, resulting in less autogenous shrinkage. The autogenous shrinkage even might be negligible compared to the drying shrinkage strains, in drying conditions. Therefore, also fitting of the drying shrinkage models to the total shrinkage results, neglecting autogenous shrinkage, is performed. The results of the model fitting are presented in Fig. 22 and the RMSE of the different models is summarized in Fig. 23.

It is observed from Fig. 22 that the same general behaviour as with the total shrinkage model fitting is noticed. The fitting of the Bazant B4 and Model Code 2010 model is worse at early ages, while at later ages the fitting of all models is quite good and almost perfect for the RC I mix. Comparing the errors of the total - and drying shrinkage model fitting (Fig. 23), it can be concluded that for the Bazant B4 and Eurocode 2 model, the error was lower for the drying shrinkage model fitting, while for the β-n model the error was lower for the total shrinkage model fitting. The error of the Model Code 2010 model of the reference mixes (RC I and RC II) was higher for the drying shrinkage model fitting, while for the CFC mixes the error was the highest for the total model fitting. However, the differences were marginal. It can thus be concluded that, similar to the total shrinkage model fitting, the β-n model appears to be the best predictor of the drying shrinkage, followed by the Eurocode 2 model for the two reference mixes and followed by the Bazant B4 model for the two CFC mixes.

5. Conclusion

The influence of the calcined dredging sediments as an SCM on the heat release, mechanical properties and shrinkage behaviour of concrete was studied experimentally and numerically. Cement replacement ratios of 20, 30 and 40 wt% CFC were considered. The main findings are summarized as follows:

- The CFC concrete mixes develop more heat than the RC II mix with fly ash, but less heat than the OPC reference mix.
- Although the strength of the CFC concrete mixes develops slower than the strength of the OPC reference mix, higher compressive strength results are obtained at later ages (> 28 days).

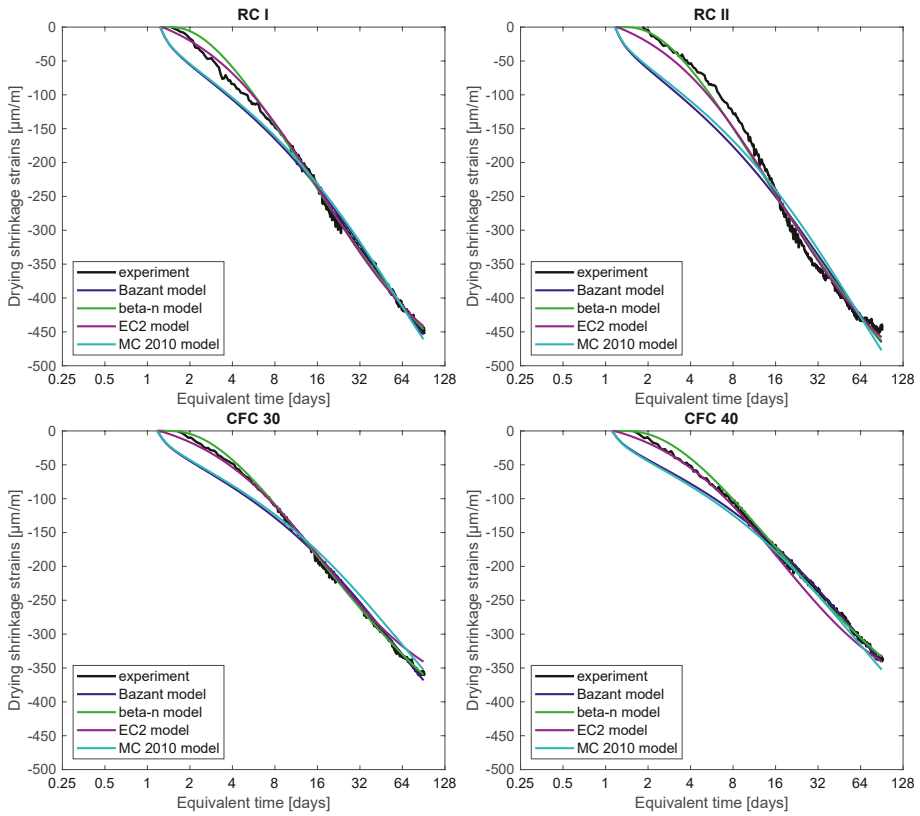

Fig. 22. Different drying shrinkage models for the different concrete mixes, compared with the experimental results.

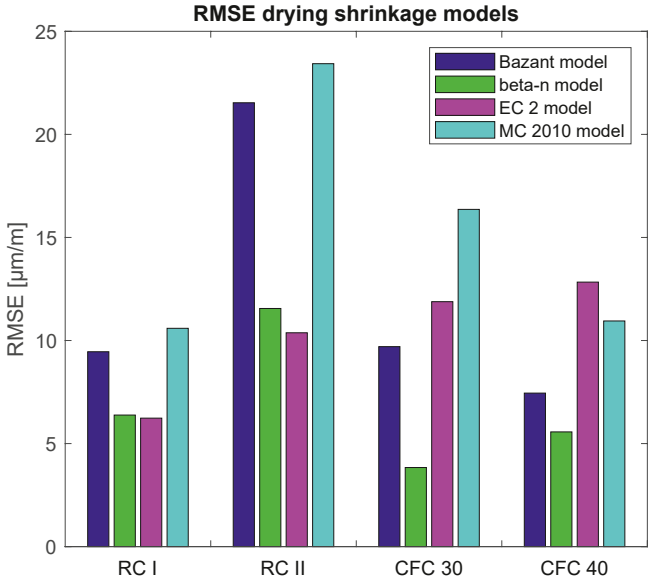

Fig. 23. RMSE of the different drying shrinkage models for the different concrete compositions.

- Both autogenous and total shrinkage are reduced by using CFC blended cement.
- The mechanical properties development model of Eurocode 2 describes well the development of the compressive strength, tensile strength and static E-modulus of the CFC concrete mixes.
- The autogenous and drying shrinkage were both modelled using existing empirical shrinkage models. The Bazant B4 model appeared to be the best prediction model for the autogenous shrinkage. The β-n model was the best predictor for the drying shrinkage, followed by the EC 2 model for the reference mixes and the Bazant model for the CFC blended cement mixes.
- Large similarities between CFC blended cement and FA blended cement are observed, regarding hydration, strength and shrinkage behaviour, proving CFC to behave as a typical SCM in concrete.

The results are promising for further research regarding creep, durability properties and cracking risk (by shrinkage restraint) of concrete with addition of CFC. Furthermore the results also support the use of CFC as SCM in concrete by providing parametrised models to predict the CFC concrete heat release, mechanical performance and dimensional changes.

Declaration of competing interest

The authors declare that they have no known competing financial interests or personal relationships that could have appeared to influence the work reported in this paper.

Acknowledgments

This study was accomplished with the support of the Flemish Government (aMT, MOW); Jos Vandekeybus and Joris Dockx are gratefully acknowledged for their support. Stéphanie Staquet and Jérôme Carette are gratefully acknowledged for the use of the BTJADE device at ULB and their help with the treatment of the results.

References

[1] K.L. Scrivener, V.M. John, E.M. Gartner, Eco-efficient cements: potential economically viable solutions for a low-CO_2 cement-based materials industry, Cement Concr. Res. 114 (2018) 2–26.
[2] M.S. Imbabi, C. Carrigan, S. McKenna, Trends and developments in green cement and concrete technology, Int. J. Sustain. Build. Environ. 1 (2) (2012) 194–216.

[3] United Nations, Bigger climate action emerging in cement industry (2019), Retrieved from, https://unfccc.int/news/bigger-climate-action-emerging-in-cement-industry, 2019, July 25.
[4] CEMBUREAU, Clinker substitution (2018), Retrieved from, https://lowcarboneconomy.cembureau.eu/5-parallel-routes/resource-efficiency/clinker-substitution/, 2019, July 25.
[5] M.C. Juenger, R. Siddique, Recent advances in understanding the role of supplementary cementitious materials in concrete, Cement Concr. Res. 78 (2015) 71–80.
[6] R.J. Flatt, N. Roussel, C.R. Cheeseman, Concrete: an eco material that needs to be improved, J. Eur. Ceram. Soc. 32 (11) (2012) 2787–2798.
[7] B.B. Sabir, S. Wild, J. Bai, Metakaolin and calcined clays as pozzolans for concrete: a review, Cement Concr. Compos. 23 (6) (2001) 441–454.
[8] T.A. Dang, S. Kamali-Bernard, W.A. Prince, Design of new blended cement based on marine dredged sediment, Construct. Build. Mater. 41 (2013) 602–611.
[9] B. Rabehi, Y. Ghernouti, K. Boumchedda, Strength and compressive behaviour of ultra high-performance fibre-reinforced concrete (UHPFRC) incorporating algerian calcined clays as pozzolanic materials and silica fume, Eur. J. Environ. Civ. Eng. 17 (8) (2013) 599–615.
[10] M.A. Chikouche, E. Ghorbel, M. Bibi, The possibility of using dredging sludge in manufacturing cements: optimization of heat treatment cycle and ratio replacement, Construct. Build. Mater. 106 (2016) 330–341.
[11] N.-E. Bouhamou, F. Mostefa, A. Mebrouki, K. Bendani, N. Belas, Influence of dredged sediment on the shrinkage behavior of self-compacting concrete, Mater. Technol. 50 (1) (2016) 127–135.
[12] R. Snellings, Ö. Cizer, L. Horckmans, P.T. Durdziński, P. Dierckx, P. Nielsen, K. Van Balen, L. Vandewalle, Properties and pozzolanic reactivity of flash calcined dredging sediments, Appl. Clay Sci. 129 (2016) 35–39.
[13] A. Faure, A. Smith, C. Coudray, B. Anger, H. Colina, I. Moulin, F. Thery, Ability of two dam fine-grained sediments to be used in cement industry as raw material for clinker production and as pozzolanic additional constituent of Portland-composite cement, Waste Biomass Valorization 8 (6) (2017) 2141–2163.
[14] R. Snellings, L. Horckmans, C. Van Bunderen, L. Vandewalle, O. Cizer, Flash-calcined dredging sediment blended cements: effect on cement hydration and properties, Mater. Struct. 50 (6) (2017) 241.
[15] C. Van Bunderen, R. Snellings, L. Vandewalle, Ö. Cizer, Early-age hydration and autogenous deformation of cement paste containing flash calcined dredging sediments, Construct. Build. Mater. 200 (2019) 104–115.
[16] R. Snellings, L. Horckmans, P. Durdzinski, C. Van Bunderen, L. Vandewalle, K. Van Balen, J. Dockx, J. Vandekeybus, Ö. Cizer, Calcined dredged sediments as supplementary cementitious materials: properties and pozzolanic reactivity, in: O. M. Jensen, K. Kovler, N. De Belie (Eds.), Proceedings of the International RILEM Conference on Materials, Systems and Structures in Civil Engineering (Segment on Concrete with Supplementary Cementitious Materials), pp. 205–212.
[17] European Committee for Standardization, Eurocode 2: Design of Concrete Structures - Part 1-1: General Rules and Rules for Buildings (EN 1992-1-1), 2005.
[18] International Federation for Structural Concrete (Fib), Model Code 2010, 2010.
[19] American Concrete Institute (A.C.I.), Guide for Modeling and Calculation Shrinkage in Hardened Concrete, 2008.
[20] Japan Society of Civil Engineers (JSCE), JSCE Guidelines for Concrete, Standard Specifications for Concrete Structures - 2007 "Design", 2010.
[21] N. J. Gardner, M. J. Lockman, Design provisions for drying shrinkage and creep of normal-strength concrete, ACI Mater. J. 98 (2).
[22] Z.P. Bazant, M. Jirásek, M. Hubler, I. Carol, RILEM draft recommendation: TC-242-MDC multi-decade creep and shrinkage of concrete: material model and structural analysis. model B4 for creep, drying shrinkage and autogenous shrinkage of normal and high-strength concretes with multi-decade applicability, Mater. Struct. 48 (4) (2015) 753–770.
[23] Z. Li, Drying shrinkage prediction of paste containing meta-kaolin and ultrafine fly ash for developing ultra-high performance concrete, Mater. Today Commun. 6 (2016) 74–80.
[24] J.M. Abdalhmid, A.F. Ashour, T. Sheehan, Long-term drying shrinkage of self-compacting concrete: experimental and analytical investigations, Construct. Build. Mater. 202 (2019) 825–837.
[25] D.W. Mokarem, R.E. Weyers, D.S. Lane, Development of a shrinkage performance specifications and prediction model analysis for supplemental cementitious material concrete mixtures, Cement Concr. Res. 35 (5) (2005) 918–925.
[26] R. Siddique, M.I. Khan, Supplementary Cementing Materials, Springer Science & Business Media, 2011.
[27] R. Snellings, G. Mertens, J. Elsen, Supplementary cementitious materials, Rev. Mineral. Geochem. 74 (1) (2012) 211–278.
[28] C. Boulay, Test rig for early age measurements of the autogenous shrinkage of a concrete, in: RILEM-JCI International Workshop ConCrack, vol. 3, 2012, pp. 111–122.
[29] J. Carette, S. Joseph, O. Cizer, S. Staquet, Decoupling the autogenous swelling from the self-desiccation deformation in early age concrete with mineral additions: micro-macro observations and unified modelling, Cement Concr. Compos. 85 (2017) 122–132.
[30] G. Heirman, L. Vandewalle, D. Van Gemert, V. Boel, K. Audenaert, G. De Schutter, B. Desmet, J. Vantomme, Time-dependent deformations of limestone powder type self-compacting concrete, Eng. Struct. 30 (10) (2008) 2945–2956.
[31] J. Carette, S. Staquet, Monitoring the setting process of eco-binders by ultrasonic p-wave and s-wave transmission velocity measurement: mortar vs concrete, Construct. Build. Mater. 110 (2016) 32–41.
[32] Y. Akkaya, C. Ouyang, S.P. Shah, Effect of supplementary cementitious materials on shrinkage and crack development in concrete, Cement Concr. Compos. 29 (2) (2007) 117–123.
[33] L. Wang, H.Q. Yang, S.H. Zhou, E. Chen, S.W. Tang, Mechanical properties, long-term hydration heat, shrinkage behavior and crack resistance of dam concrete designed with low heat portland (LHP) cement and fly ash, Construct. Build. Mater. 187 (2018) 1073–1091.
[34] X. Hu, Z. Shi, C. Shi, Z. Wu, B. Tong, Z. Ou, G. De Schutter, Drying shrinkage and cracking resistance of concrete made with ternary cementitious components, Construct. Build. Mater. 149 (2017) 406–415.
[35] S. Tangtermsirikul, H9: Effect of Chemical Composition and Particle Size of Fly Ash on Autogenous Shrinkage of Paste, CRC Press, London, 1999, pp. 175–185.
[36] P. Termkhajornkit, T. Nawa, M. Nakai, T. Saito, Effect of fly ash on autogenous shrinkage, Cement Concr. Res. 35 (3) (2005) 473–482.
[37] A.K. Saha, Effect of class F fly ash on the durability properties of concrete, Sustain. Environ. Res. 28 (1) (2018) 25–31.
[38] A. Asselin, Early-age Cracking in Massive Concrete Structures: Sensitivity Analysis and Parameters Identification, Tech. rep., École Normale Supérieure Paris-Saclay, 2017/2018.
[39] F. Benboudjema, J.-M. Torrenti, Early-age behaviour of concrete nuclear containments, Nucl. Eng. Des. 238 (10) (2008) 2495–2506.
[40] M. Briffaut, F. Benboudjema, J.-M. Torrenti, G. Nahas, Concrete early age basic creep: experiments and test of rheological modelling approaches, Construct. Build. Mater. 36 (2012) 373–380.
[41] F.-J. Ulm, O. Coussy, Couplings in early-age concrete: from material modeling to structural design, Int. J. Solid Struct. 35 (31) (1998) 4295–4311.
[42] J. Zreiki, F. Bouchelaghem, M. Chaouche, Early-age behaviour of concrete in massive structures, experimentation and modelling, Nucl. Eng. Des. 240 (10) (2010) 2643–2654.
[43] M. Cervera, J. Oliver, T. Prato, Thermo-chemo-mechanical model for concrete. I: hydration and aging, J. Eng. Mech. 125 (9) (1999) 1018–1027.
[44] T. Kanstad, T.A. Hammer, Ø. Bjøntegaard, E.J. Sellevold, Mechanical properties of young concrete: Part II: determination of model parameters and test program proposals, Mater. Struct. 36 (4) (2003) 226–230.
[45] A. Darquennes, F. Benboudjema, Behavior of Activated Ternary Binders under Autogenous Condition, vol. 326, ACI Symposium Publication, 2018, 22.1–22.10.
[46] B. Klemczak, M. Batog, M. Pilch, Assessment of concrete strength development models with regard to concretes with low clinker cements, Arch. Civ. Mech. Eng. 16 (2) (2016) 235–247.
[47] F. Rifai, Immobilisation de déchets magnésiens dans un matériau alcali-activé: étude expérimentale et numérique, Ph.D. thesis, 2017.